Describing the SAXS Profile of Unilamellar Liposomes via Beating Waves

Laura Baraldi, Serena. R. Alfarano, Flavia Sousa, Raffaele Mezzenga, Barbara Rothen-Rutishaser, Alke Petri-Fink, Sandor Balog*

Corresponding author

Sandor Balog - Adolphe Merkle Institute, University of Fribourg, Chemin des Verdiers 4, 1700 Fribourg, Switzerland; Email: sandor.balog@unifr.ch

Author

Laura Baraldi - Adolphe Merkle Institute, University of Fribourg, Chemin des Verdiers 4, 1700 Fribourg, Switzerland and Dipartimento di Scienze Chimiche, della Vita e della Sostenibilità Ambientale, Università di Parma, 43124 Parma, Italy; Email: laura.baraldi@unipr.it

Serena R. Alfarano - Department of Health Sciences and Technology, ETH Zürich, Zürich 8092, Switzerland; Email: serenarosa.alfarano@hest.ethz.ch

Flavia Sousa - Adolphe Merkle Institute, University of Fribourg, Chemin des Verdiers 4, 1700 Fribourg, Switzerland; Email: flavia.sousa@unifr.ch

Raffaele Mezzenga - Department of Health Sciences and Technology, ETH Zürich, Zürich 8092, Switzerland; Email: raffaele.mezzenga@hest.ethz.ch

Barbara Rothen-Rutishaser - Adolphe Merkle Institute, University of Fribourg, Chemin des Verdiers 4, 1700 Fribourg, Switzerland; Email: barbara.rothen@unifr.ch

Alke Petri-Fink - Chemistry Department, University of Fribourg, Chemin du Musée 9 and Adolphe Merkle Institute, University of Fribourg, Chemin des Verdiers 4, 1700 Fribourg, Switzerland; Email: alke.fink@unifr.ch

Keywords: SAXS, liposome, lipid bilayer, mathematical modeling

Abstract

Unilamellar liposomes are spherical vesicles that can transport and deliver drugs. Here, we present a straightforward mathematical model that describes the features of small-angle X-ray scattering (SAXS) from unilamellar liposomes.

The COVID pandemic has taught us many lessons, and we might face other rapidly spreading infectious diseases in the future,[1-3] owing to increasing population, worldwide commerce, globetrotting, sedentary lifestyle, massive consumption of meat, microplastics in the environment, and waterborne diseases resulting from global warming. Consequently, pharmaceutical R&D must be even faster in responding to unforeseen scenarios. These days, nearly 600 liposomal formulations are in ongoing clinical trials,[4] and ensuring quality in production scalability[5] and characterization[6] are significant bottlenecks. Differently speaking, developing a successful formulation requires synthetic excellence and efficient characterization and purification.[7]

Liposomes are the first generation of lipid nanoparticles (LNP). Since their discovery in 1965,[8] liposomes (i.e., phosphatidylcholine lipid vesicles) have been used to deliver drugs, such as small molecules and nucleic acids,[9] as

biocompatible formulations.[10] They comprise an aqueous core and one or more hydrophobic shells composed of a head-tail-tail-head phospholipid bilayer. This structural arrangement can encapsulate hydrophilic and lipophilic drugs and drugs at the interface between the aqueous core and the bilayer.[11] Their popularity arises from the ability to protect the drug from degradation and effectively deliver it exactly where needed, thus reducing side effects.[12] Over the years, much progress has been made in developing liposomal formulations. Many targets have been made reachable, addressing different pathologies—such as cancer, pain, and infections—by tailoring the composition and functionalizing the surface of the liposomes.[13] For instance, ionizable cationic lipids can be enrolled to interact with labile solutes like mRNA and then actively trigger their release inside the cell.[14] This formulation strategy saved many lives during the COVID pandemic, where the mRNA coding for the coronavirus spike protein was entrapped into lipid-based colloidal particles to produce vaccines.[15] Like most colloidal soft matter, liposomes are dynamic systems[15,16] sensitive to external stimuli.[16] Accordingly, liposomes must be characterized in their native state, under ambient or physiological conditions, in situ, and in a noninvasive / non-destructive manner. Particle size and size distribution may be readily characterized via, e.g., dynamic and static light scattering.[17] Characterizing the structural features of the membrane-like lipid bilayer, however, requires sub-nanometer resolution and high statistical power,[18] and small-angle X-ray scattering (SAXS) is the first-choice experimental technique.[19]

SAXS is a conceptually simple technique:[20] the dispersion of the lipid particles is irradiated with a narrow and collimated beam of quasi-monochromatic soft X-rays—photon wavelength is roughly between 0.1-10 nm—which interacts quasi-elastically with the dispersion. The X-rays scattered off the particles are detected with a position-sensitive area detector. The intensity of scattering as a function of the scattering angle (referred to as scattering pattern) is a function of the volumetric distribution of the electrons (referred to as electron density) within the atomic/molecular bricks making up the lipid formulation. Thus, the scattering pattern is characteristic of the atomic/molecular arrangement of matter on the nanoscale and carries information about the orientation, shape, and size of domains. From a mathematical perspective, the recorded scattering pattern is proportional to the square of the three-dimensional Fourier transform of the electron density distribution $\rho(\bar{r})$ in the material, $I(\bar{q}) \propto |\mathrm{FT}\ \rho(\bar{r})|^2$, and thus, by analyzing the SAXS profile, information on the nanoscale structure and morphology of the sample studied may be quantified. In case of liposomes, $|\mathrm{FT}\ \rho(\bar{r})|^2$ may be referred to as the form factor: $S(\bar{q}) = |\mathrm{FT}\ \rho(\bar{r})|^2$.[21] The angular dependence is defined through the so-called scattering vector, whose amplitude is $q = 4\pi/\lambda \sin\theta/2$, where θ is the scattering angle and λ the wavelength. Thus, SAXS provides information on the nanoscale structure and morphology of the sample studied, typically on the 100 nm-1nm length scale.

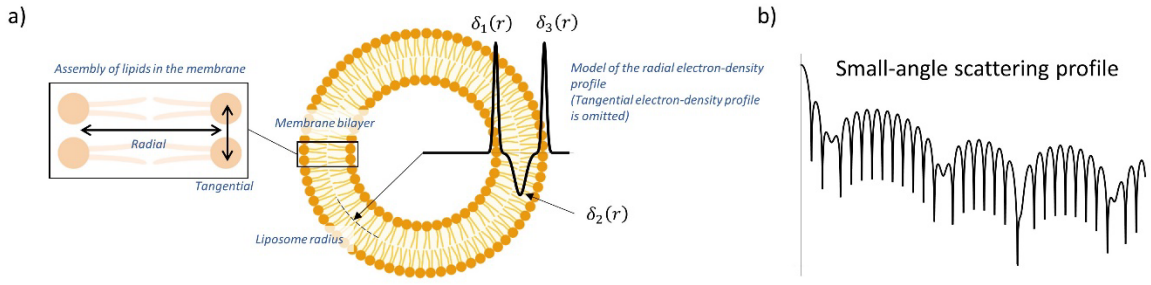

Figure 1. a) Illustration of the cross-sectional structure of spherical and symmetric lipid membranes. Such spherical and uni-lamellar assembly exhibits two main symmetries: one in the radial direction, and the other in the tangential direction, as indicated by the arrows. The tangential profile represents circular/spherical stacking of lipids, which is usually omitted in SAXS analysis of membrane thickness.

This works, as most works, addresses the radial profile. The solid line—drawn as the sum of three Gaussian functions—$\delta(r) = \sum_{i=1}^{3} \delta_i(r)$, two for the heads and one for tails of the lipids—shows a plausible mathematical model of the radial profile of the bilayer electron density. b) Scattering profile: The square of the Fourier transform of the radial profile ($\delta(r)$, Eq 1) contains quantitative information about the membrane structure, and is directly measurable via SAXS.

The Fourier transform is essentially an integral over the scattering volume $\mathrm{FT}\,\rho(\bar{r}) = \int \rho(\bar{r})\, e^{i\cdot\bar{q}\cdot\bar{r}} d\bar{r}$. By using spherical coordinates, where the electron density is expressed as a function of the radial distance (r), azimuthal angle $d\theta$ and polar angle $d\varphi$, this integral is written as

1) $$\mathrm{FT}\,\rho(\bar{r}) = \int_0^{2\pi}\int_0^{\pi}\int_0^{\infty} \rho(r,\theta,\varphi)\cdot r^2\cdot\sin\theta\cdot e^{i\cdot q\cdot r\cdot\cos\theta} dr\, d\theta\, d\varphi.$$

Figure 1 shows an idealized structural sketch of a spherical lipid membrane. Phospholipids are a class of lipids made of three main structural components: a polar head group, a nonpolar tail, and a glycerol backbone. The polar head is hydrophilic, while the nonpolar tail is hydrophobic. The backbone connects the head and the tail. The electron densities of these components are different, and therefore SAXS may be used to study how lipids are assembled. In an aqueous environment, liposomes exhibit a relatively well-defined membrane-like shell: The head groups face towards the aqueous environment, both inside and outside, and the tails are oriented inwards. According to this view, one may define a tangential and a radial electron density profile. Given that the interest lays mostly in characterizing the radial bilayer profile, most of the time it is implicitly assumed that the systematic head-to head variation in the tangential profile is negligible, and thus, quasi constant, which may be an adequate approximation, because the spherical assembly of the lipids (as discrete units) shows a high-degree of rotational symmetry with respect to θ and φ. Accordingly, it may be approximated as being isotropic, i.e., $\rho(r,\theta,\varphi)$ is not a function of θ and φ: $(\bar{r}) = \rho(r,\theta,\varphi) = \rho(r)$. This assumption greatly simplifies the evaluation of Equation 1, because two integrals, the one in φ and the one in θ, simply becomes 2π and $2\,\mathrm{sinc}(q\cdot r)$, respectively. Accordingly, in the case of spherical symmetry (isotropy), the three-dimensional Fourier transform may be expressed by one single integral

2) $$\mathrm{FT}\,\rho(\bar{r}) = 4\pi\int \rho(r)\cdot\mathrm{sinc}(q\cdot r)\, r^2 dr,$$

where $\rho(r)$ is an isotropic radial function that embodies the electron density profile of the structure across the bilayer. Seminal works—using X-rays and showing for the first time that lipid membranes feature a bilayer that may interact with, e.g., proteins—were carried out early in the 70s.[22-27] The nano-scale radial structure was found to exhibit a systematic variation in the electron density profile across the membrane, which consist of two peaks separated by a broad dip. The first feature is attributed to the head groups of high-electron density and the latter to the fatty chains of low-electron-density. This structural view still defines the current mainstream in the analysis of SAXS spectra,[21,28] and, $\rho(r)$ is most frequently modeled by the sum of at least three gaussian functions (Figure 1a), two for the polar heads, and one for the tails and backbone

3) $$\rho(r) = \sum_{i=1}^{3} \rho_i(r)$$

where $\rho_i(r)$ stands for a regular Gaussian function with a mean μ_i, variance σ_i^2, and amplitude a_i

4) $$\rho_i(r) = a_i \frac{e^{\frac{(r-\mu_i)^2}{2\sigma_i^2}}}{\sqrt{2\pi}\sigma_i}.$$

Integration in Equation 2 is a linear operation, therefore Equation 3 may be evaluated as

5) $$\mathrm{FT}\,\sum_{i=1}^{3} \rho_i(r) = \sum_{i=1}^{3} \mathrm{FT}\,\rho_i(r).$$

Evaluating the Fourier transform of a Gaussian function yields a closed-form expression

6) $\mathrm{FT}\,\rho_i(r) = A_i\,(f_i + g_i)$

where $A_i = 4\pi \cdot a_i \cdot e^{-\frac{1}{2}q^2\sigma_i^2}$, $f_i = \sin(\mu_i \cdot q)\,\frac{\mu_i}{q}$, $g_i = \cos(\mu_i \cdot q) \cdot \sigma_i^2$. One now can express the structure factor:

7) $\mathrm{FT}\,\delta(r) = \sum_{i=1}^{3} \mathrm{FT}\,\delta_i(r) = \sum_{i=1}^{3} A_i\,(f_i + g_i)$

and

8) $S(q) = \left|\sum_{i=1}^{3} A_i\,(f_i + g_i)\right|^2$.

Equation 8 operates only on real-valued numbers, and by using the properties of the absolute value function ($|x| = \sqrt{x^2}$), one may rewrite Equation 8

9) $S(q) = \left(\sum_{i=1}^{3} A_i\,(f_i + g_i)\right)^2$.

What remains is accounting for the fact that liposomes exhibit size polydispersity, which necessitates an integration of Equation 9 over the distribution of liposome radius:

10) $S(q) = \int p(r)\,S(q,r)dr$.

Equation 10 does not yield a solution in closed form but may be evaluated numerically. Describing the size distribution $p(r)$ involves at least two additional parameters: mean radius and standard deviation of the radius. Accordingly, if the bilayer is not symmetric, one has 11 parameters in total. Nonetheless, this parametric model is conceptually very elegant, and the so-called forward problem, that is, predicting the SAXS spectrum from a known electron-density radial function of liposomes, is straightforward via Equation 1-10. Figure 2 shows a representative set of simulated scattering spectra of two symmetric bilayers with systematically varied radius. The liposome radius is defined at the global minimum of the radial profile (Figure 1a). One may identify two dominant features in the SAXS spectra: the first, is a rapid oscillatory function that is modulated by a second and slowly varying envelope function. The rapid oscillations relate to particle radius and vanish upon size polydispersity. With polydispersity, the scattering spectra approaches the envelope of the structure factor.

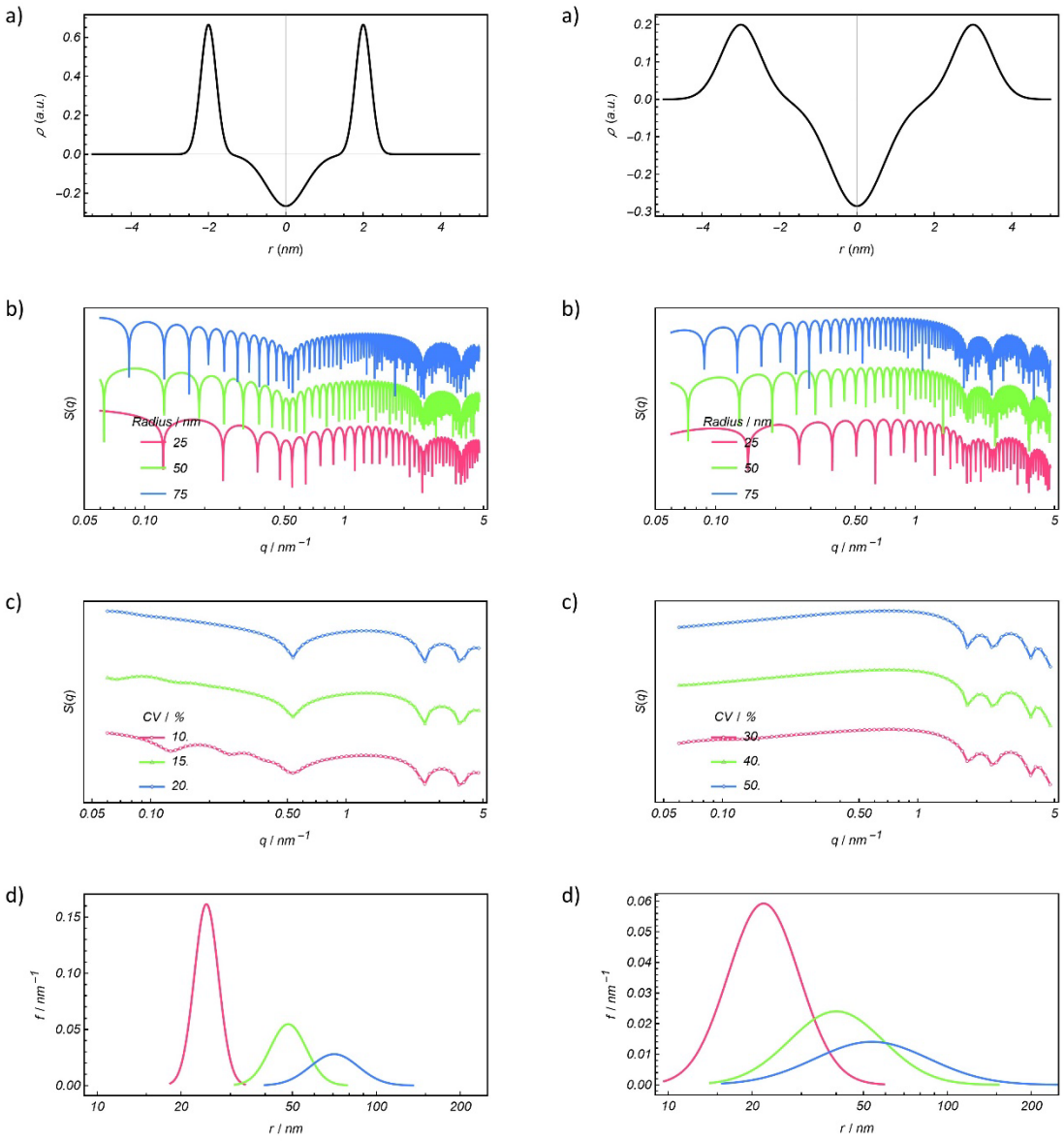

Figure 2. Scattering spectra computed via Equation 1-10. a) Simulation of two arbitrary symmetric radial profiles of liposomes, and b) the corresponding scattering spectra with different radii. While the spectra are seemingly complex, one may identify two dominant features: 1) a rapid oscillatory function that is modulated by 2) a slowly varying envelope function. c) The rapid oscillations, which are related to particle radius, vanish upon increasing polydispersity in the radius, and the scattering spectra approaches the envelope of the structure factor. CV, the coefficient of variation, is defined as the ratio of the standard deviation and the mean. d) Corresponding lognormal distributions of the radius modelling polydispersity.

Doing this transformation backward, which is referred to as the inverse problem, is much more difficult, and a solution usually requires deep domain-specific knowledge. Given that the model may be amenable to parametric analysis, most of the time, $\rho(r)$ is modeled explicitly, and the model evaluated and regressed against experimental SAXS spectra. In this way, one can infer the model's parameters, and thus characterize the structure of the studied bilayer. However, even the simplest gaussian model comes with nine parameters, three amplitudes, three centers, and three widths. In the case of symmetric membranes, nine reduces to six. If size polydispersity is considered, the number of regression parameters

increases according to the complexity of the size distribution. Commercial and free computational tool dedicated to the analysis of small-angle scattering spectra have been made available,[29-33] yet the mathematical apparatus, both analytical and numerical, might be well beyond the expertise of most scientist concerned with the development of novel lipid formulations. Indeed, in our experience, obtaining a physically meaningful and converging solution of the inverse problem has been proven to be highly uncertain, and by using freely available computational tools, we failed to analyze even well-defined idealized synthetic spectra.

Here we set out to develop a simple yet useful alternative in SAXS analysis on lipid bilayer membranes. We focus on two aspects: 1) we aim at an approach that considerably decreases the complexity of the analysis, yet 2) it infers the features of the parametric model of the membrane electron-density profile with a good statistical accuracy. For this, we will focus on deriving and utilizing the envelope function. The envelop function is not an exact solution, but it is a very good approximation considering the practical limitations—such as noise, dynamic range (q-range), and resolution—of most SAXS data recorded on lab-scale instruments. The fact that SAXS spectra are rather insensitive to the size and polydispersity of liposomes, and the structural information about the bilayer profile is carried only by the envelope of the spectra (Figure 2b and c) was pointed-out already in 1975,[34] yet, to the best of our knowledge, the relevance in the SAXS analysis of liposomes has never been recognized nor deployed. We show here that this approach is both straightforward and beneficial.

Equation 4 describes the gaussian models of the radial profile, and Equation 9 describes the structure factor. The radius and the thickness of the membrane of the application-relevant liposomes are such that $\mu_i/q \gg \sigma_i^2$, over the q-range of the SAXS spectra.[21] As a consequence, $f_i \gg g_i$, and thus one can truncate the expression: $f_i + g_i \cong f_i$. Thus, Equation 6 and 9 simplify: $\mathrm{FT}\,\delta_i(r) \cong A_i\, f_i$ and

11) $S(q) \cong (\sum_{i=1}^{3} A_i\, f_i)^2$.

A simple computational series (similarly to Figure 2) can prove that omitting the term g_i will not change the observable spectra, as the difference resulting from having or not having the term g_i in the structure factor is well below the noise-level of experimental spectra.

The truncated version given by Equation 11 encourages us to look at the structure factor from another angle and consider it as the amplitude of the linear superstition of three harmonic waves. After all, SAXS essentially relies on a well-known wave phenomenon: interference of coherent waves. An important aspect to recognize is the fact that the membranes of such liposomes are thin, that is, $|\mu_i - \mu_j| \ll \mu_i$. In other words, the frequencies of the harmonic waves are very close to one another. This proximity of spatial frequencies, and the superposition of harmonic waves having slightly different frequencies results in a special wave phenomenon: beating waves (Figure 3).[35]

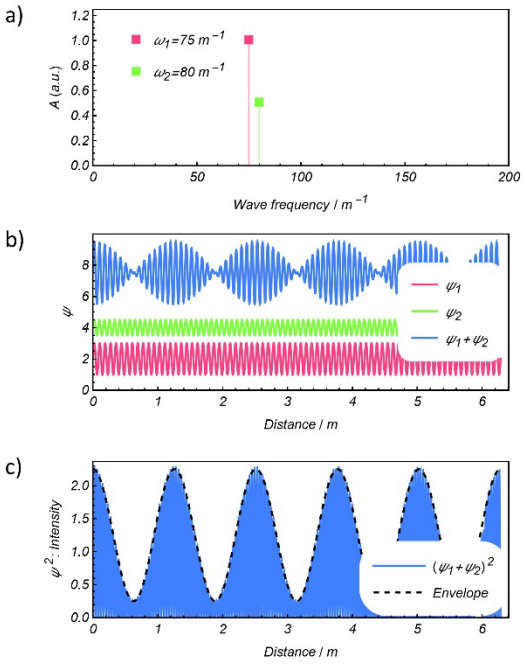

Figure 3. Beating of two superposing harmonic waves. a) The frequency and amplitudes of two harmonic waves, and b) their waveform: $\psi_i = A_i \cdot \sin(\omega_i \cdot x)$. (The waveforms are shifted vertically for the sake of visibility.) The linear superposition of the waves with slightly different frequencies form beats, which appear as a slow harmonic modulation of the amplitude of the rapid oscillations. The frequency of this modulation (the beat frequency) is solely defined by the difference of the two frequencies: $\omega_B = |\omega_1 - \omega_2|$. c) The intensity of the superposing waves is covered by an envelope function: $f_E(x) = {A_1}^2 + {A_2}^2 + 2A_1A_2 \cdot \cos(\omega_B \cdot x)$.

In fact, what we can observe in Figure 2b is the same wave phenomena resulting from the superposition of three waves: $\sum_{i=1}^{3} A_i f_i$, and the envelope function is the intensity beats of the three superposing waves. It is easy to show that for N harmonic waves with amplitudes A_i and frequency ω_i, the envelope function is given by:

12) $$f_E(x) = \sum_{i=1}^{N} {A_i}^2 + 2\sum_{i=1}^{N-1}\sum_{j>i}^{N} A_i A_j \cdot \cos(\omega_{ij} \cdot x)$$

where the respective beat frequencies are $\omega_{ij} = |\omega_i - \omega_j|$. In our case, we can now apply Equation 12 to describe SAXS spectra if liposome membranes, where according to the gaussian model, each wave is composed of an amplitude and a harmonic term with frequency μ_i:

13) $$4\pi \cdot a_i \cdot e^{-\frac{1}{2}q^2\sigma_i^2}\ \mu_i/q \times \sin(\mu_i \cdot q)$$

Using Equation 13 and 14, Equation 12 is easily evaluated and provides a closed form for describing the SAXS spectra of unilamellar liposomes:

14) $$\frac{1}{q^2}\sum_{i=1}^{3} a_i^2 \cdot \mu_i^2 \cdot e^{-q^2\sigma_i^2} + \frac{1}{q^2}\Big(2a_1a_2\mu_1\mu_2 e^{-\frac{1}{2}q^2(\sigma_1^2+\sigma_2^2)} \cos(q(\mu_2-\mu_1)) + 2a_1a_3\mu_1\mu_3 e^{-\frac{1}{2}q^2(\sigma_1^2+\sigma_3^2)} \cos(q(\mu_3-\mu_1)) + 2a_2a_3\mu_3\mu_3 e^{-\frac{1}{2}q^2(\sigma_2^2+\sigma_3^2)} \cos(q(\mu_3-\mu_3))\Big).$$

We believe that Equation 14 may be a basis of a simple yet useful alternative in SAXS analysis on lipid bilayer membranes, and thus, advance the characterization of liposomal drug delivery systems.

Acknowledgements

Financial support was given by the Adolphe Merkle Institute, the University of Parma, and the National Center of Competence in Research (NCCR) for Bio-Inspired Materials at the University of Fribourg.

References

(1) Edwards, A. M.; Baric, R. S.; Saphire, E. O.; Ulmer, J. B. Stopping Pandemics before They Start: Lessons Learned from Sars-Cov-2*, Science,* **2022**, *375*, 1133-1139.

(2) Behl, A.; Nair, A.; Mohagaonkar, S.; Yadav, P.; Gambhir, K.; Tyagi, N.; Sharma, R. K.; Butola, B. S.; Sharma, N. In *Infection, Genetics and Evolution*; Elsevier B.V., 2022.

(3) Edelson, P. J.; Harold, R.; Ackelsberg, J.; Duchin, J. S.; Lawrence, S. J.; Manabe, Y. C.; Zahn, M.; LaRocque, R. C. Climate Change and the Epidemiology of Infectious Diseases in the United States*, Clinical infectious diseases : an official publication of the Infectious Diseases Society of America,* **2023**, *76*, 950-956.

(4)

(5) Liz-Marzán, L. M.; Nel, A. E.; Brinker, C. J.; Chan, W. C. W.; Chen, C.; Chen, X.; Ho, D.; Hu, T.; Kataoka, K.; Kotov, N. A.; Parak, W. J.; Stevens, M. M. In *ACS Nano*; American Chemical Society, 2022, pp 13257-13259.

(6) Fan, Y.; Marioli, M.; Zhang, K. Analytical Characterization of Liposomes and Other Lipid Nanoparticles for Drug Delivery*, Journal of Pharmaceutical and Biomedical Analysis,* **2021**, *192*, 113642.

(7) Dimov, N.; Kastner, E.; Hussain, M.; Perrie, Y.; Szita, N. Formation and Purification of Tailored Liposomes for Drug Delivery Using a Module-Based Micro Continuous-Flow System*, Scientific Reports,* **2017**, *7*.

(8) Bangham, A. D.; Standish, M. M.; Watkins, J. C. Diffusion of Univalent Ions across the Lamellae of Swollen Phospholipids*, Journal of Molecular Biology,* **1965**, *13*, 238-252.

(9) Tenchov, R.; Bird, R.; Curtze, A. E.; Zhou, Q. In *ACS Nano*; American Chemical Society, 2021, pp 16982-17015.

(10) Gregoriadis, G.; Ryman, B. E. Fate of Protein-Containing Liposomes Injected into Rats: An Approach to the Treatment of Storage Diseases*, European Journal of Biochemistry,* **1972**, *24*, 485-491.

(11) Large, D. E.; Abdelmessih, R. G.; Fink, E. A.; Auguste, D. T. In *Advanced Drug Delivery Reviews*; Elsevier B.V., 2021.

(12) Sesarman, A.; Muntean, D.; Abrudan, B.; Tefas, L.; Sylvester, B.; Licarete, E.; Rauca, V.; Luput, L.; Patras, L.; Banciu, M.; Vlase, L.; Porfire, A. Improved Pharmacokinetics and Reduced Side Effects of Doxorubicin Therapy by Liposomal Co-Encapsulation with Curcumin*, Journal of Liposome Research,* **2021**, *31*, 1-10.

(13) Kapoor, M.; Lee, S. L.; Tyner, K. M. Liposomal Drug Product Development and Quality: Current Us Experience and Perspective*, AAPS Journal,* **2017**, *19*, 632-641.

(14) Lou, G.; Anderluzzi, G.; Schmidt, S. T.; Woods, S.; Gallorini, S.; Brazzoli, M.; Giusti, F.; Ferlenghi, I.; Johnson, R. N.; Roberts, C. W.; O'Hagan, D. T.; Baudner, B. C.; Perrie, Y. Delivery of Self-Amplifying Mrna Vaccines by Cationic Lipid Nanoparticles: The Impact of Cationic Lipid Selection*, Journal of Controlled Release,* **2020**, *325*, 370-379.

(15) Gregoriadis, G. Liposomes and Mrna: Two Technologies Together Create a Covid-19 Vaccine*, Medicine in Drug Discovery,* **2021**, *12*, 100104-100104.

(16) Prakash K Soni, T. R. S. Purification of Drug Loaded Liposomal Formulations by a Novel Stirred Cell Ultrafiltration Technique, *Pharmaceutical Nanotechnology,* **2021**, 347-360.

(17) Danaei, M.; Dehghankhold, M.; Ataei, S.; Hasanzadeh Davarani, F.; Javanmard, R.; Dokhani, A.; Khorasani, S.; Mozafari, M. R. In *Pharmaceutics*; MDPI AG, 2018.

(18) Heberle, F. A.; Pabst, G. In *Biophysical Reviews*; Springer Verlag, 2017, pp 353-373.

(19) Dong, Y.-D.; Boyd, B. J. Applications of X-Ray Scattering in Pharmaceutical Science, *International Journal of Pharmaceutics,* **2011**, *417*, 101-111.

(20) Li, T.; Senesi, A. J.; Lee, B. Small Angle X-Ray Scattering for Nanoparticle Research, *Chemical Reviews,* **2016**, *116*, 11128-11180.

(21) Brzustowicz, M. R.; Brunger, A. T. X-Ray Scattering from Unilamellar Lipid Vesicles, *Journal of Applied Crystallography,* **2005**, *38*, 126-131.

(22) Levine, Y. K.; Wilkins, M. H. F. Structure of Oriented Lipid Bilayers, *Nature New Biology,* **1971**, *230*, 69-72.

(23) Wilkins, M. H. F.; Blaurock, A. E.; Engelman, D. M. Bilayer Structure in Membranes, *Nature New Biology,* **1971**, *230*, 72-76.

(24) Blaurock, A. E. Locating Protein in Membranes, *Nature,* **1972**, *240*, 556-557.

(25) Blaurock, A. E. X-Ray Diffraction Pattern from a Bilayer with Protein Outside, *Biophysical Journal,* **1973**, *13*, 281-289.

(26) Atkinson, D.; Hauser, H.; Shipley, G. G.; Stubbs, J. M. Structure and Morphology of Phosphatidylserine Dispersions, *Biochimica et Biophysica Acta (BBA) - Biomembranes,* **1974**, *339*, 10-29.

(27) Blaurock, A. E.; Lieb, W. R. X-Ray Diffraction Studies of Biomembranes, *Nature,* **1975**, *255*, 370-371.

(28) Bouwstra, J. A.; Gooris, G. S.; Bras, W.; Talsma, H. Small Angle X-Ray Scattering: Possibilities and Limitations in Characterization of Vesicles, *Chemistry and Physics of Lipids,* **1993**, *64*, 83-98.

(29) Ilavsky, J.; Jemian, P. R. Irena: Tool Suite for Modeling and Analysis of Small-Angle Scattering, *Journal of Applied Crystallography,* **2009**, *42*, 347-353.

(30) Bressler, I.; Kohlbrecher, J.; Thunemann, A. F. Sasfit: A Tool for Small-Angle Scattering Data Analysis Using a Library of Analytical Expressions, *Journal of Applied Crystallography,* **2015**, *48*, 1587-1598.

(31) Konarev, P. V.; Petoukhov, M. V.; Dadinova, L. A.; Fedorova, N. V.; Volynsky, P. E.; Svergun, D. I.; Batishchev, O. V.; Shtykova, E. V. Bilmix: A New Approach to Restore the Size Polydispersity and Electron Density Profiles of Lipid Bilayers from Liposomes Using Small-Angle X-Ray Scattering Data, *Journal of Applied Crystallography,* **2020**, *53*, 236-243.

(32) Lewis-Laurent, A.; Doktorova, M.; Heberle, F. A.; Marquardt, D. Vesicle Viewer: Online Visualization and Analysis Of small-Angle Scattering from Lipid Vesicles, *Biophysical Journal,* **2021**, *120*, 4639-4648.

(33) Manalastas-Cantos, K.; Konarev, P. V.; Hajizadeh, N. R.; Kikhney, A. G.; Petoukhov, M. V.; Molodenskiy, D. S.; Panjkovich, A.; Mertens, H. D. T.; Gruzinov, A.; Borges, C.; Jeffries, C. M.; Svergun, D. I.; Franke, D. Atsas 3.0: Expanded Functionality and New Tools for Small-Angle Scattering Data Analysis, *Journal of Applied Crystallography,* **2021**, *54*, 343-355.

(34) Moody, M. F. Diffraction by Dispersion of Spherical Membrane Vesicles. I. The Basic Equations, *Acta Crystallographica Section A,* **1975**, *31*, 8-15.
(35) Radi, H. A.; Rasmussen, J. O. In *Principles of Physics: For Scientists and Engineers*, Radi, H. A.; Rasmussen, J. O., Eds.; Springer Berlin Heidelberg: Berlin, Heidelberg, 2013, pp 531-560.